Available online at www.sciencedirect.com
SCIENCE DIRECT
Talanta 68 (2006) 504–515
Talanta
www.elsevier.com/locate/talanta

Determining salinity using a multimode fiber optic surface plasmon resonance dip-probe

Darcy J. Gentleman [a], Karl S. Booksh [b,*]

[a] *Department of Chemistry, University of Toronto, Toronto, Ont., Canada*
[b] *Department of Chemistry and Biochemistry, Arizona State University, Main Campus, P.O. Box 871604, Tempe, AZ 85287-1604, USA*

Received 23 June 2004; received in revised form 16 September 2004; accepted 16 September 2004
Available online 22 June 2005

Abstract

For the first time a fiber optic surface plasmon resonance sensor with demonstrated accuracy and precision of less than 200 ppm salinity is presented for calibration across a range of temperatures and salinities. Also shown is the potential for the sensor system to reach precisions of 10 ppm or less. Calibration models are constructed for 28–48‰ salinity and a method for translating the calibration models to account for varying temperatures between 0 and 25 °C are demonstrated. The long-term susceptibility of the fiber optic sensor to fouling and drift is discussed.

Keywords: Hydrothermal vents; Practical salinity scale; Refractive index; Ocean density; Fiber optic sensors

1. Introduction

1.1. Why measure salinity with refractive index sensors?

Density (salinity), temperature and pressure (depth) are the fundamental parameters for the seawater equation of state, which is essential to climate models [1]. Because seawater is an aqueous solution of dissolved salts, salinity is the standard measurement used to determine the density of ocean water [2]. Prior to 1967, the standard method of determining salinity was through titration of chloride-dominated seawater against silver nitrate, with an accuracy of 30 ppm [2]. Conductivity was touted as a possible salinometric technique, but it was not standardized until 1967 when conductometric sensors attained a precision and accuracy exceeding that of the chemical technique [3]. The conductivity–salinity scale was further revised in 1978 to account for the advent of portable conductivity-temperature-depth (CTD) sensors used in field monitoring with high-precision/accuracy bench-top thermosalinographs [3,4]. This practical salinity scale of 1978 (PSS 78), further recognized by UNESCO in 1980, is now so universal in the oceanographic determination of density that salinity is used almost synonymously for density in references [1,5]. The accuracy of PSS 78 is 1 ppm, with a precision of <1 ppm [4]. It should be noted PSS 78 uses "Practical Salinity Units" or PSU, as the measurement is based on a ratio of standard seawater to the sample and is therefore inherently unitless. For this paper, salinity will be reported in either ‰ or ppm KCl, the former of which is essentially the same as PSU.

Conductivity cannot account for species that may add to seawater's density but do not measurably conduct electricity and is compositionally dependent due to heterovalency [5]. When conductivity was being standardized in the 1960s, the use of refractive index (RI) to determine salinity was suggested [6]. However, the precision and accuracy of conductometric sensors developed faster than refractometric sensors, the former of which were also made portable more easily. Recently, meticulous statistical treatment of

* Corresponding author. Tel.: +1 4809653058; fax: +1 4809652747.
E-mail address: kbooksh@asu.edu (K.S. Booksh).

0039-9140/$ – see front matter © 2005 Elsevier B.V. All rights reserved.
doi:10.1016/j.talanta.2004.09.029

salinity–density data sets has shown that RI correlates to density 80% better than conductivity [7]. Interferometric refractometers can achieve sub-1 ppm accuracy, but are inherently bench-top devices that require strict temperature control in their surrounding environment to at least ±0.1 °C [6]. Thus, refractometric determination of seawater density tends to be limited to exacting studies where sample-capture is acceptable. Climatological research depends on density information to track global ocean circulation, an application for which 10–100 ppm is an acceptable sensitivity [8,9]. Therefore, a refractometric sensor that can attain a sub-100 ppm sensitivity while being robust enough for field deployment would find itself useful in salinity/densitometry.

1.2. State of the art in fiber optic refractive sensors for oceanography

Chemical oceanography has become increasingly attracted to the use of fiber optic based sensors [10]. The flexible nature of fiber optics, combined with their relatively low fabrication cost, makes them attractive to any field where in situ remote sensing is desirable. A fiber optic system can also miniaturize many table-top optical systems, bringing the possibility of in situ refractometry to the ocean. Several groups have attained accuracies between 1000 and mid-100 ppm using various fiber optic systems [11–13]. The best sensitivity reported is that by Zhao et al., with precision of ±300 ppm using a miniaturized differential refractometer [14–16]. Zhao et al. estimate their spectral resolution gives a sensitivity of 12 ppm. Their design requires a saline standard and a prism in the sensor head, so the potential to miniaturize the sensor is limited.

Surface plasmon resonance (SPR) is another technique that measures RI changes, and has been successfully used with fiber optics in environmental systems in recent years [17–23]. SPR spectroscopy can be employed to determine RI when light in a waveguide is attenuated following excitation of a surface plasmon on a thin metallic film deposited on the waveguide. In the case of a fiber optic waveguide, there need be no prisms or moving parts in the sensor tip. Therefore, such sensors can be <200 μm diameter at the tip and inexpensive. At a minimum, such a sensor could be mated next to a traditional conductivity/temperature (CTD) probe for in situ ocean salinity monitoring and the two sensors used in concert to better characterize the density of seawater.

Three groups have used FO-SPR to measure salinity; however, none of these three studies calibrated the sensors across a range of temperatures. Grunwald and Holst have attained a sensitivity of 1000 ppm using a multimode fiber with a tapered tip [24,25]. Liu et al., using a multimode fiber, report an RI sensitivity of 8.9×10^{-5} RIU and claim this corresponds to a salinity sensitivity of 10 ppm [25]. However, based on the accepted values for RI change with salinity of $\sim 3 \times 10^{-7}$ RIU/ppm, [6,27] the sensitivity of Liu et al.'s sensor is closer to 450 ppm. Lastly, Esteban et al., using a single mode system report a sensitivity of 100 ppm, as their SPR data tracked with conductivity probe good to 100 ppm [20].

1.3. Our relationship to the state of the art

In order for an SPR salinity probe to be useful in the field, its performance must be demonstrated both over a range of salinities and temperatures. The RI of seawater changes monotonically from 0‰ to 42‰ and monotonically from −1 to 32 °C at typical ocean salinities. However, a sensor is unlikely to encounter this full range of salinities and temperatures in a given deployment. The fiber optic system under development here is envisioned for two particular applications. First is the stationary deployment near deep-sea hydrothermal vents where the goal is to monitor the diffusion of vent fluid. In these applications, thermal equilibrium is rapidly achieved, but fluid mixing and diffusion is spatially varied with predominant currents. The second application is drop sensing where the probe would rapidly collect data while descending to the ocean floor. Here the probe will possibly encounter thermoclines and haloclines. Laboratory experiments chosen to test this sensor have been designed to present a significantly greater range of salinities than would be expected in most applications and a comparable range of temperatures that would be encountered for a given field experiment. This paper shows the fiber optic based SPR dip-probe (FO-SPR) can achieve salinity predictions of <200 ppm with a precision of at least 100 ppm over several temperatures and salinities of marine relevance. This result is in the same range as the isothermal 100 ppm reported by Esteban et al. [20]. Both data sets relied on conductivity probes with sensitivities of 100 ppm at best. Thus, it is believed that with better calibration, these small and inexpensive FO-SPR sensors could achieve sensitivities of <100 ppm, rendering them useful to field studies of the ocean.

Our laboratory has demonstrated the ability to make reproducible flat-polished tip FO-SPR sensors for use in aqueous systems [19,28,29]. Sensing tips are constructed from 400 μm core optical fibers, and are typically less than 5 cm in length. Connection to a light source and spectrometer is achieved with fiber optic "jumpers," thus the sensor apparatus can be easily multiplexed and adapted for remote use. Studies with aqueous sucrose have shown correlating the λ_{SPR} with bulk RI or analyte concentration are sensitive and robust enough for quantitative applications [29]. Previous studies in our laboratory suggested a prediction of salinity over of <1000 ppm several temperatures was attainable with this sensor [29]. The current study improved on the experimental design by collecting conductivity and temperature data simultaneously with the SPR spectra in temperature controlled solutions of aqueous KCl. A limit of determination based on observed prediction errors of at least 200 ppm and a precision of <100 ppm is attainable with these FO-SPR sensors. The potential to deliver accuracy and precision of <100 ppm is foreseeable with a more powerful, less portable, spectrometer and CCD camera.

2. Apparatus

A computer-controlled pumping system was created to facilitate mixing of saline solutions and collect data from the FO-SPR sensor, a thermistor, and a conductivity cell. A Pentium 3 laptop (Dell) with a 1.1 GHz processor and 256 Mb of RAM, connected to a dedicated docking station, was used for control data collection and processing.

2.1. SPR sensor

The manufacture and optimization of the FO-SPR probes used in this study has been described in detail elsewhere [19]. All probes were made from 400 μm core diameter FT400EMT silica fiber (3 M) with a TECS™ cladding and TEFZEL™ buffer. A 7-cm piece of fiber is cut and 10 mm of cladding and buffer near the fiber's tip is removed mechanically. The tip is then polished using standard lapping films. A 2-nm film of Cr is sputtered in a 208HR evaporation deposition chamber (Cressington) on the flat tip, followed by 50 nm of Au. The Cr is applied to ensure the Au will adhere to the surface. This mirror is further protected by replacing the buffer on just the last 3–5 mm of the fiber tip, then dipping the tip in epoxy. Next, the fiber is epoxied into an SMA coupler. Once the epoxy has cured, the cladding is removed from the exposed part of the shaft using acetone on a Kimwipe™. The probe is then reintroduced to the sputtering chamber to be covered with the 2 nm Cr undercoat and the 50-nm Au layer. Rotating wheels installed in the chamber enable uniform sputtering on this cylindrical surface. Fig. 1 shows a cross-section schematic of this probe and a scaled photograph. Seven such probes were prepared in one batch and the two with the shortest required exposure times (best light return) were selected for use in the experiment.

A quartz–tungsten–halogen (QTH) lamp (Oriel) was the light source. A bifurcated optical fiber jumper made of FT400EMT silica fiber (same as the probes) coupled light from the source to the probe and on to the spectrometer. An HR2000 spectrometer (Ocean Optics) was the detector, with a spectral resolution of 0.2 nm/pixel. The spectrometer was connected to the computer through a USB port and dedicated software collected spectra consisting of 10 averaged frames every 5.8 s. As soon as an air standard for the FO-SPR probe was collected, the probe was submerged in the mixing chamber. If removal was required due to maintenance during the experiment, the probe was kept in deionized water for the duration and then re-immersed. The probes were in deionized water for <0.8% of the total experiment time.

2.2. Conductivity

Conductivity measurements were made with a YSI 3253 small volume four-wire conductivity cell and a dedicated 3200 m (YSI). The meter reported a resolution of 0.01 mS

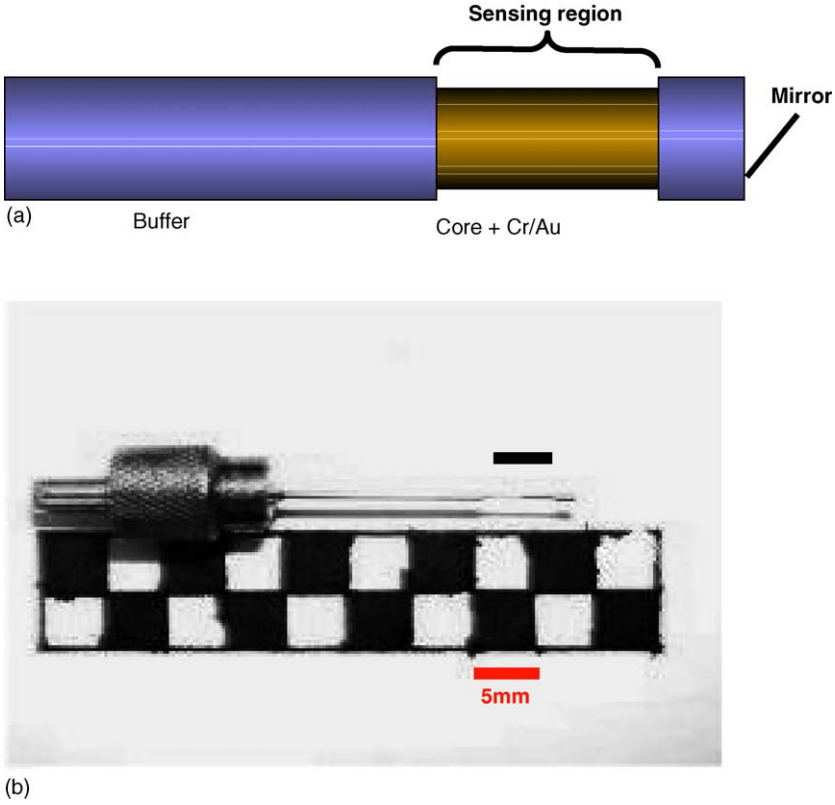

Fig. 1. The FO-SPR probe used for this paper. (a) Shows cross-sectional schematic of the probe. Both the mirror and the sensing region have the 2 nm Cr undercoat and a 50 nm Au covering. Photo in (b) shows a typical probe. Though neither of those used herein. Line over probe shows sensing region.

with an accuracy of ±1.0%. The cell constant was calibrated using commercial standard solutions of KCl at 10,000 and 100,000 μS/cm (VWR/Control Company) as per the YSI manual's instructions. The cell constant, calculated as 0.913/cm, was internally applied to the conductance reading. A thermistor included in the probe had a resolution of 0.01 °C and an accuracy of ±0.1%. The meter reports "salinity" but does not use PSS 78 for this calculation, and therefore was only used as a qualitative check against the reported conductivity for experimental progress checks. The temperature correction was disabled to permit the later combination of the conductivity probe's measured temperature and conductivity using PSS 78. Data was streamed every 5 s from the meter to the computer through an RS 232 port and collected using the Hyperterminal accessory in MS Windows 2000.

2.3. Temperature

A YSI 55036 glass-bead thermistor (YSI) was selected to measure temperature given its ability to be calibrated to a precision of 0.001 °C. Ten such thermistors were baked for 1 week at 400 °C to settle out their long-term thermal drift. Thermistors were fitted with banana plugs to be hooked up to a $6\frac{1}{2}$ digit Keithley 2000 digital multimeter (Keithley). Success of the baking was then established through thermal shocking by rapid switching between two immersion temperature standards: isopropyl alcohol and dry ice at −40 °C and boiling water at 100 °C. Thermistors whose resistance readings settled out within 20 cycles were selected for calibration. The thermistor head was protected after shock treatment by wrapping it in PTFE tape and Parafilm™.

Thermistor calibration was performed through immersion of the thermistor affixed to a mass of Cu, wrapped in Al foil, in an Isotherm 3013 circulation bath (Fisher/Ness Labs) containing a 50/50 mixture of ethylene glycol and water. The bath displays to 0.01 °C and is accurate to 0.02 °C, according to its manual. A plasticized Styrofoam block 3 cm think covered the open bath to insulate it from ambient thermal fluctuations. Five temperatures between 1 and 32 °C were used, with the bath given 24 h to achieve thermal equilibrium. Twenty resistance measurements taken at increments of 30 s by hand were then used for each temperature for fitting to the Steinhard equation using LINEST in MS Excel:

$$T = [A + B \ln R + C(\ln R)^3]^{-1} \quad (1)$$

where T is in Kelvin and R is the resistance. The thermistor used for the experiments had a precision of 0.002 °C with an R^2 of 0.99996 for $n = 100$.

The thermistor was immersed in the mix chamber to the same depth as the sensing region of the FO-SPR. As these thermistors have a head diameter of ∼3 mm, it is easy to get the tip of the FO-SPR and the thermistor within 5 mm of each other without their touching. The FO-SPR sensor was not long enough to be immersed to the same depth as the conductivity probe. Therefore, the temperatures collected by the conductivity probe were used in the PSS 78 calculation. This assumes the salinity within the mix chamber is constant, given the stir bar's constant mixing and ensuring a tight seal in the chamber's lid through the use of Parafilm™. Conversely, thermal gradients in a circulation bath of this type are inevitable, thus the temperatures used for the spectral data were those collected by the thermistor, immersed to the same depth as the FO-SPR.

Readings were collected by the Keithley multimeter using the "slow" rate collection on its display with a moving average of 100 readings. The measurement cycle was approximately 500 ms. The multimeter was connected to the computer through a standard GPIB port, and was queried every 5 s by a LabVIEW 6.1 program (National Instruments).

2.4. Saline solutions

$KCl_{(aq)}$ solutions were prepared according to the standard method for making salinometric standards [2]. To ensure total dryness, KCl (EM Scientific/KGaA Merck) was placed in an oven at 800 °C and allowed to melt in a clean ceramic crucible. Approximately, 3 h were required to melt 80 g of $KCl_{(s)}$. The molten KCl was then quickly poured onto a clean stainless steel sheet and allowed to cool. The glassy KCl was then weighed to an amount appropriate to make either a 42.000‰ or 70.000‰ solution with deionized water (Millipore) in a 1000.0 mL volumetric flask. As the experiments required several litres of solution in total, a new solution would be made as needed, typically once per week. As concentration (salinity) was determined in the experiment using conductivity, the changing concentration in the $KCl_{(aq)}$ reservoir was not an issue.

The $KCl_{(aq)}$ solution and deionized water were placed in 800 mL plastic reservoirs intended for cell culturing (VWR). Holes were drilled in the caps of the reservoirs to permit removal of their content with pumps, and the addition of more solution through Tygon tubing and glass funnels. All points open to the atmosphere were sealed with Parafilm™ when not in use. Temperature control was achieved by submerging and securing the reservoirs and sample chamber in the circulation bath used for the thermistor calibration.

The sample chamber consisted of a 130 mL HDPE bottle used to deliver $KCl_{(aq)}$ conductivity standards. Holes were drilled in its lid to permit insertion of leads from the pumps and the measuring probes. An aluminum foil sheath was wrapped around the bottle to prevent the ethylene glycol/water solution from contaminating the analyte. A 1-cm magnetic stir bar was placed inside the bottle, driven by an immersible stir-bar platform (VWR).

Two 50-μL LPLA2410550L constant volume electromotive pumps (The Lee Co.) were used to deliver solution to the sample chamber. Computer control was achieved through a circuit board connected through a DAQ6024E controller card (National Instruments). A LabVIEW 6.1 user interface controlled the pumps, and was not automated. The pumps could be set to either 1 or 2 Hz cycles, delivering 50 μL each cycle,

resulting in flow rates of either 3 or 6 mL/min. Solution was removed from the mixing chamber using the same line connected to that of the $KCl_{(aq)}$ pump and delivered to waste.

3. Method

3.1. Experiment 1

This first experiment tested the ability of the SPR probe to work at fairly constant temperature (±0.05 °C) across a wide range of salinities (28–42‰ KCl). Temperature was set at least 12 h in advance of an experimental series to ensure thermal equilibrium of all components were attained. Temperatures from −1 to 32 °C were randomized for collection of data at 34 different temperatures over a period of ∼40 days. The two reservoirs contained deionized water and ∼42‰ $KCl_{(aq)}$, respectively.

Prior to each measurement set, the chamber was drained using the pumps and refilled with 120.00 mL of $KCl_{(aq)}$ to a starting salinity of ∼42‰, as read by the salinity field on the conductivity meter. Upon this filling, data streaming of conductivity (κ), temperature (T) and spectra (λ_{SPR}) was recommenced. Every 30 min, 5.00 mL was drained from the chamber using a pump, and random combined volumes of deionized water and 42‰ $KCl_{(aq)}$ was flowed in to replace the 5.00 mL. Twenty such sets were collected over a period of 10 h, with no random injected concentration repeated. Upon completion, all data collected was digitally archived, and the bath was set to the next temperature.

Measurements were collected until it was determined the sensor had become insensitive to changes in salinity. This occurred after 21 days.

3.2. Experiment 2

In order to assess the sensor's ability to respond to salinities changing by more than 1.0‰ or 2.0‰, a second experiment was performed with a new probe. Prior to the measurement set, the chamber was drained with the pumps and refilled to a starting concentration as close to 35.0‰ (average open-ocean salinity) as possible. The reservoirs were thus filled with deionized water and 70.0‰ $KCl_{(aq)}$. Data streaming of κ, T and λ_{SPR} was commenced upon filling to 35.0‰.

As described below, Experiment 1 a 1-week equilibrium time was needed to achieve the best results from the SPR sensor. Therefore, prior to beginning Experiment 2, the FO-SPR

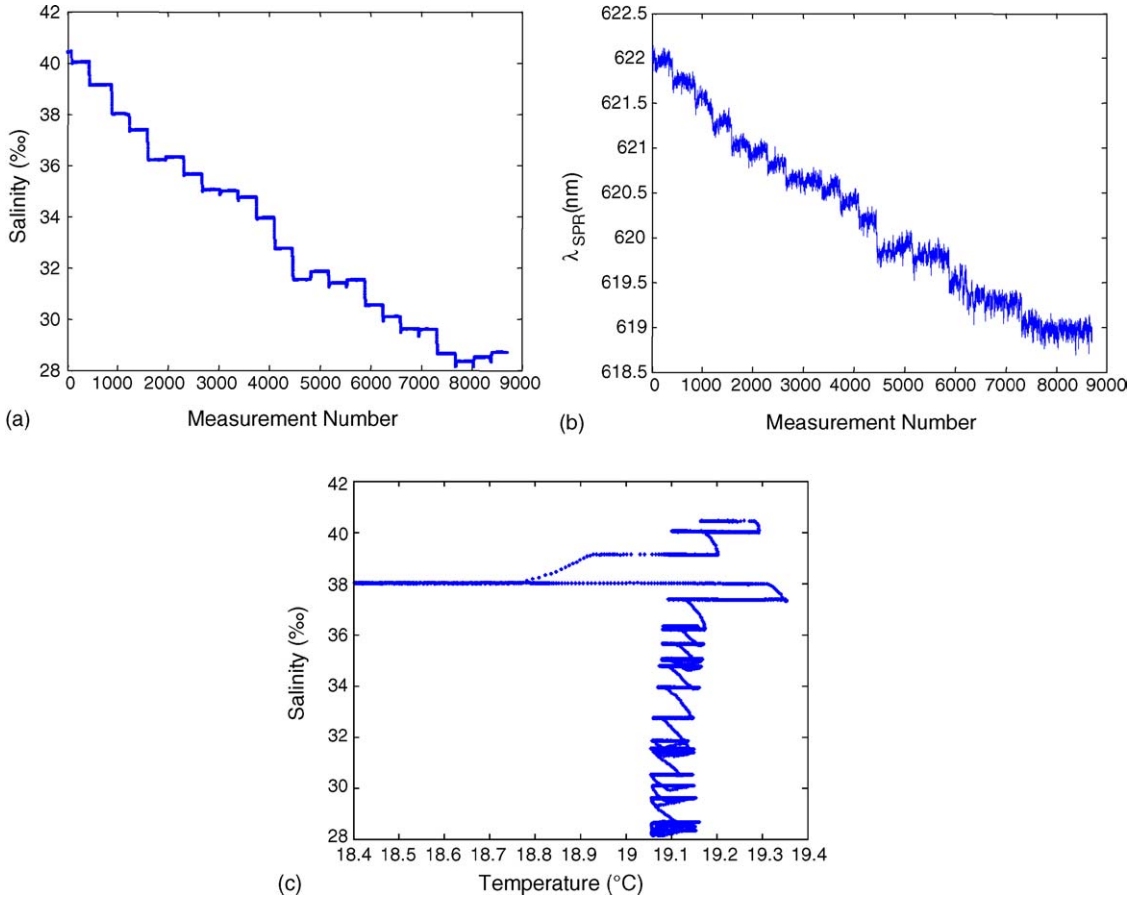

Fig. 2. Representative set from Experiment 1. Salinity shown in (a), position of λ_{SPR} in (b). Evidently the SPR signal tracks well with salinity. Using the range of temperatures covered for a given salinity from (c), data may be appropriately selected to determine prediction error.

probe was immersed in 35.0‰ $KCl_{(aq)}$ at 15 °C until no sensor drift at constant κ and T occurred. Ten random salinities between 32.0‰ and 38.0‰ were chosen and the volumes needed to drain and then replace with either deionized water or 70.0‰ $KCl_{(aq)}$ were generated. Once the salinity was achieved, the set point on the bath was raised 1.00 °C from its set value, and allowed 30 min to equilibrate. The temperature was then returned to its starting value at which time a new salinity was acquired. Ten such sets were collected. The temperatures used in this set were 14.50, 1.50, 24.50, 7.50, 19.50 °C, and one set oscillating between 13.50 and 16.50 °C.

Following this last temperature set, the conductivity probe began to report readings that did not correlate with the volumetrically estimated salinity within the chamber. Therefore, the experiment was terminated at this time.

4. Results and discussion

A sensitivity of at least 200 ppm is attainable using an FO-SPR sensor to measure salinity. This sensitivity was demonstrated for temperatures between 0 and 25 °C, and a range of salinities between 28‰ and 42‰ (∼28 and ∼42 PSU). Comparing to the previously reported values in the literature, 200 ppm approaches the lower reported, that of Esteban et al. [20] However, while that study merely showed their SPR signal tracked with their conductivity data, the present study shows with statistically significant data sets the sensitivity is attainable for several temperatures and salinities. Also, the Esteban probe is more difficult to manufacture and work with, as it requires the shaft instead of the tip of a fiber to be polished down. In order to better establish the sensitivity of FO-SPR, further work with a higher resolution spectrometer, a more accurate conductivity probe, and a greater degree of temperature control must be performed. The sensor also drifts with time to the point of losing its ability to reliably detect salinity changes over a period of days to a week. The nature of this drift must be determined and prevented to allow long-term use of the sensor both in calibration studies and field use.

All salinities were calculated from the conductivity and temperature measurements made by the YSI conductivity cell, and converted into salinity using PSS 78 equations provided by Fofonoff [1] and using MatLab R12 (MathWorks). Propagating differences in computer timing for the three collected data streams resulted in the spectral data sets often being the smallest in number of recorded measurements. Temperature data was collected every 5.0 s, conductivity

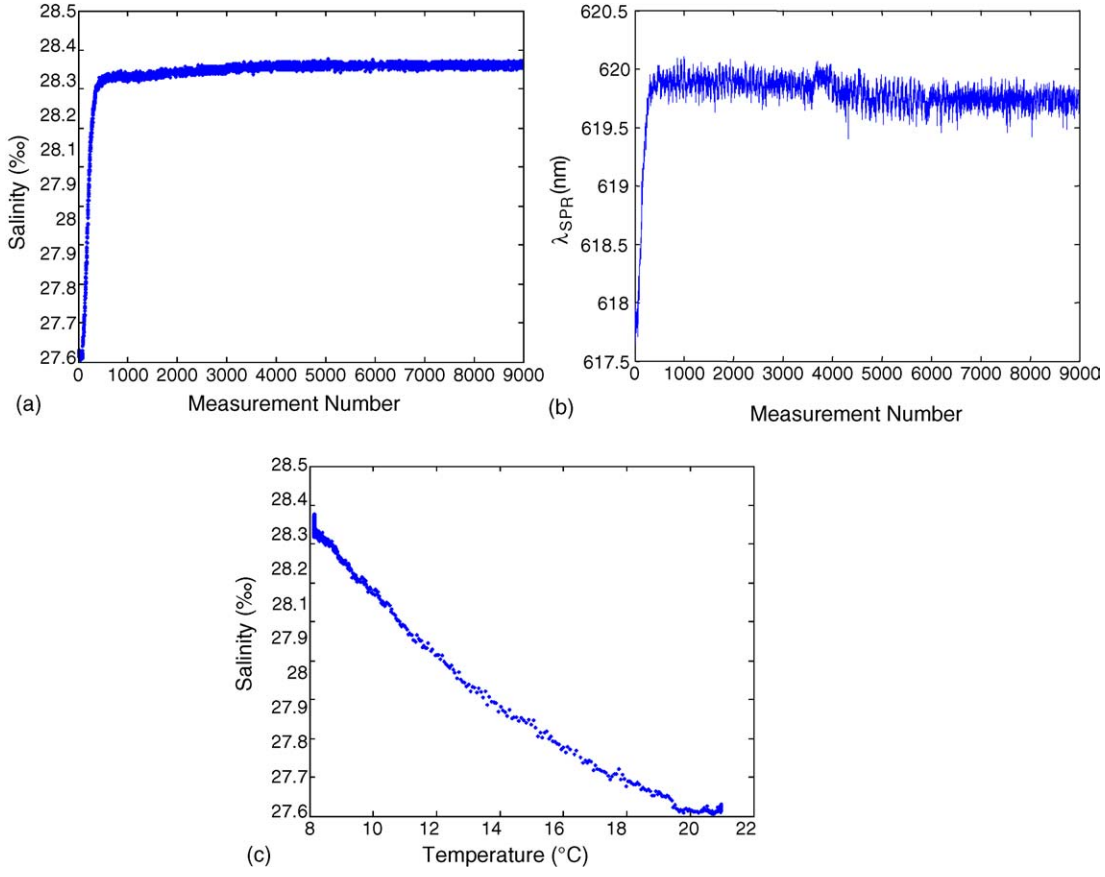

Fig. 3. Representative set from Experiment 1 while temperature was equilibrating. Salinity shown in (a), position of λ_{SPR} in (b). The plot in (c) shows the most points at the lowest temperature, indicating this run had temperature decreasing. As plot (b) shows a slight decrease in λ_{SPR}, again it shows the ability of SPR to track changing RI.

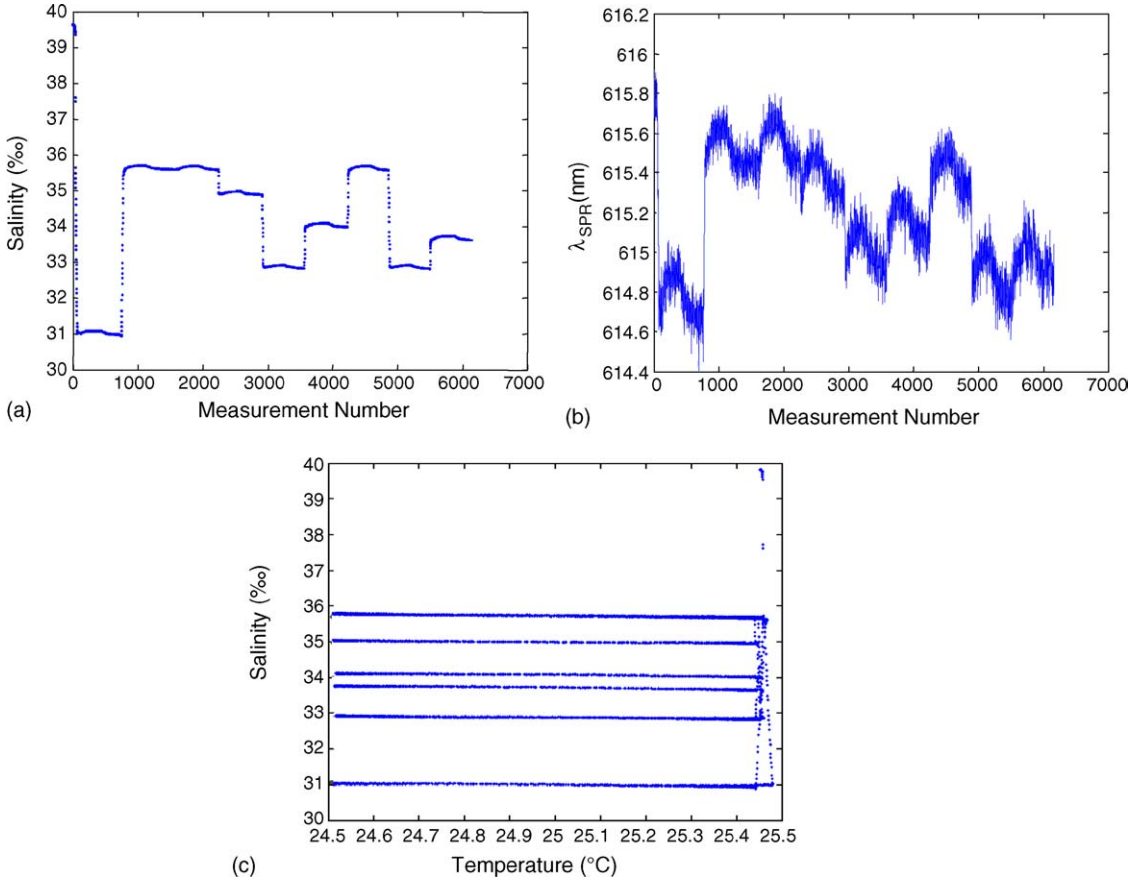

Fig. 4. Representative set from Experiment 2. Salinity shown in (a), position of λ_{SPR} in (b). As in Fig. 3 the range of salinities and temperatures covered shown in (c) allows selection for application to the prediction model.

~5.2 s and λ every 5.8 s. As the statistical studies required all sets have the same number of data points, the larger sets were linearly interpolated into the smaller sized set by a weighted average over time. Therefore, no data was lost.

Representative plots of the three types of data are shown in Figs. 2–4. Fig. 2 shows Experiment 1 during a dilution, Fig. 3 shows Experiment 1 during a temperature equilibration, and Fig. 4 shows 1 day's experimental collection from Experiment 2. In all cases, (a) shows the salinity over the course of the run, (b) shows the corresponding SPR minima and (c) shows the range of temperatures encountered for a given salinity.

4.1. Simultaneous calibration over a range of salinities and temperatures

In order to determine the sensor's ability to predict the salinity of an unknown sample across a range of temperatures, a transferable linear regression model was generated for a given range of temperatures. Separate linear calibration models were calculated to relate salinity to λ_{SPR} for the two temperatures at the extremes of calibration range. A transfer model was then calculated to adapt the linear calibration model to any temperature within the overall calibration range where T_1 and T_2 are two bounding temperature, each with an independent calibration model. The transfer model assumes the slopes (m) and intercepts (b) of the regression model between these bounding temperatures track linearly with temperature. The weighting parameter

$$p = \frac{T_{unk} - T_1}{T_2 - T_1} \tag{2}$$

allows

$$b_{unk} = b_1 + p(b_2 - b_1) \tag{3}$$

and

$$m_{unk} = m_1 + p(m_2 - m_1) \tag{4}$$

The root mean square error of prediction (RMSEP) indicates the absolute difference between predicted and true salinity (S):

$$\text{RMSEP} = \sqrt{\frac{\sum_{i=1}^{n}(S_{predicted} - S_{true})}{n}} \tag{5}$$

Fig. 5 shows trend of λ_{SPR} versus salinity across a 0.040 °C temperature variation and the absolute error of the prediction against salinity and temperature for a subset of data within Fig. 2. Note there is no trend in the errors of prediction with

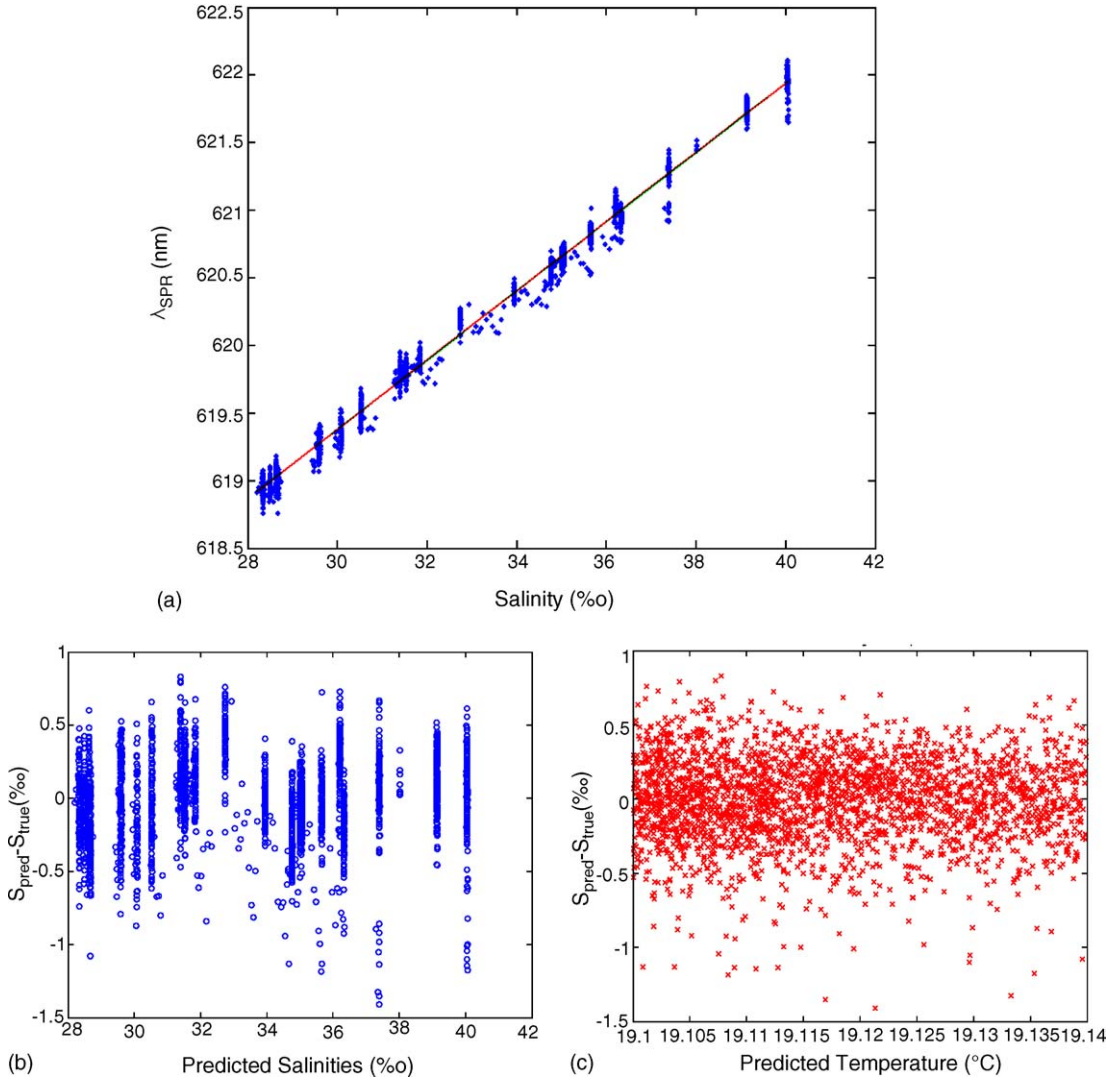

Fig. 5. Regression plots and absolute errors of prediction for a set within Fig. 2. (a) Shows the trend for λ_{SPR} vs. salinity for measurements collected between for 19.100 and 19.140 °C. The absolute error of prediction against salinity is shown in (b) and against temperature in (c). No methods were used to remove outliers as appear in (b) or (c).

respect to salinity or temperature; therefore the spread of the data is assumed to be due to thermal noise and spectral scatter.

Fig. 6 shows the RMSEP for all data (grey bars) and after exclusion of suspected outliers (black bars). The ordinate axis presents sample runs with mean temperatures between −1 and 25 °C in the order that they were recorded. The salinity calibration model was constructed over a range of ±1‰ salinity. Most of the samples demonstrated similar error structures to the data presented in Fig. 5b and c, where for a much larger calibration range, the vast majority of the predictions are accurate to within ±0.5‰ salinity. However a small fraction of the errors are relatively large. Here, the larger errors are also biased low in prediction. These outliers were identified by a Student's *t*-test (99% confidence with infinite degrees of freedom) with the standard deviation estimated from the entire population. Consequently, between 2% and 5% of the data were excluded per data set. The differences in the RMSEP with and without outliers highlights the profound effect these few samples have on the overall performance metric. Once the outliers were removed, The FO-SPR probe used in Experiment 1 was sensitive to changes in salinity of <200 ppm over several temperatures, and <300 ppm for eight or the nine data sets.

Preliminary analysis of data collected across greater temperature variations ±0.5 °C, across 32–38‰ salinity, demonstrated RMSEP of 190, 180, 380 and 130 ppm for 5, 15, 2 and 8 °C, respectively. Repeating the 15 °C analysis with a second conductivity cell to determine salinity yielded a 360 ppm RMSEP. The first cell failed after these four sample sets; it has been immersed in salt water for 6 weeks straight at this point. Fig. 7a and b present the RMSEP over 28–48‰ salinity, a significantly wider range than would be expected in most ocean environments. In general 300–600 ppm accuracy is achieved. The larger error for the sample near 0 °C (Fig. 7a)

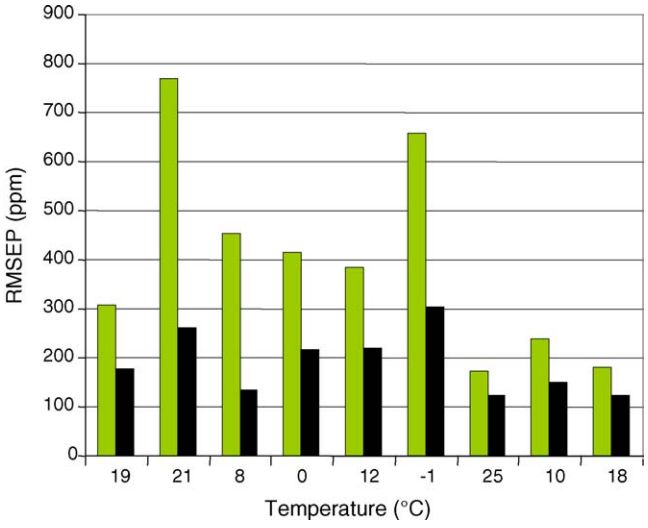

Fig. 6. RMSEP of the median (grey) and the mean below the median (black) for the indicated temperatures in Experiment 1. Each day was broken into increments of 1‰ and the predictions performed within these salinity blocks. The mean RMSEP is below 300 ppm virtually everywhere, with the majority below 200 ppm.

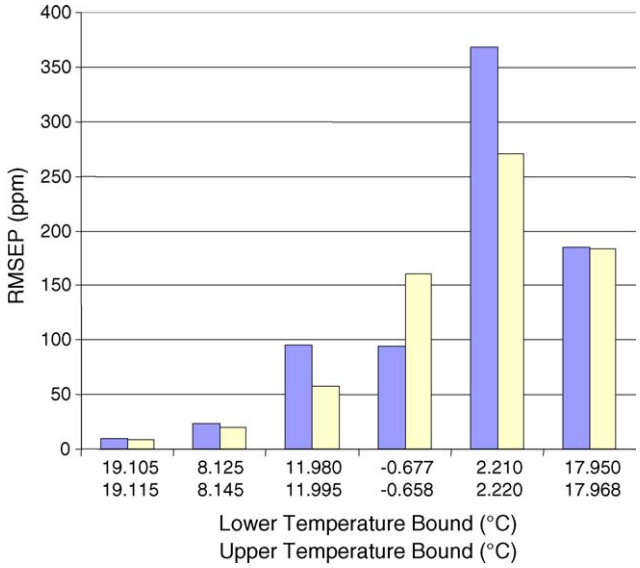

Fig. 8. RMSEP for temperature equilibration portions of Experiment 1. These results indicate a precision of <50 ppm is attainable. The dark bar is individual data point, the light bar is that of the moving average.

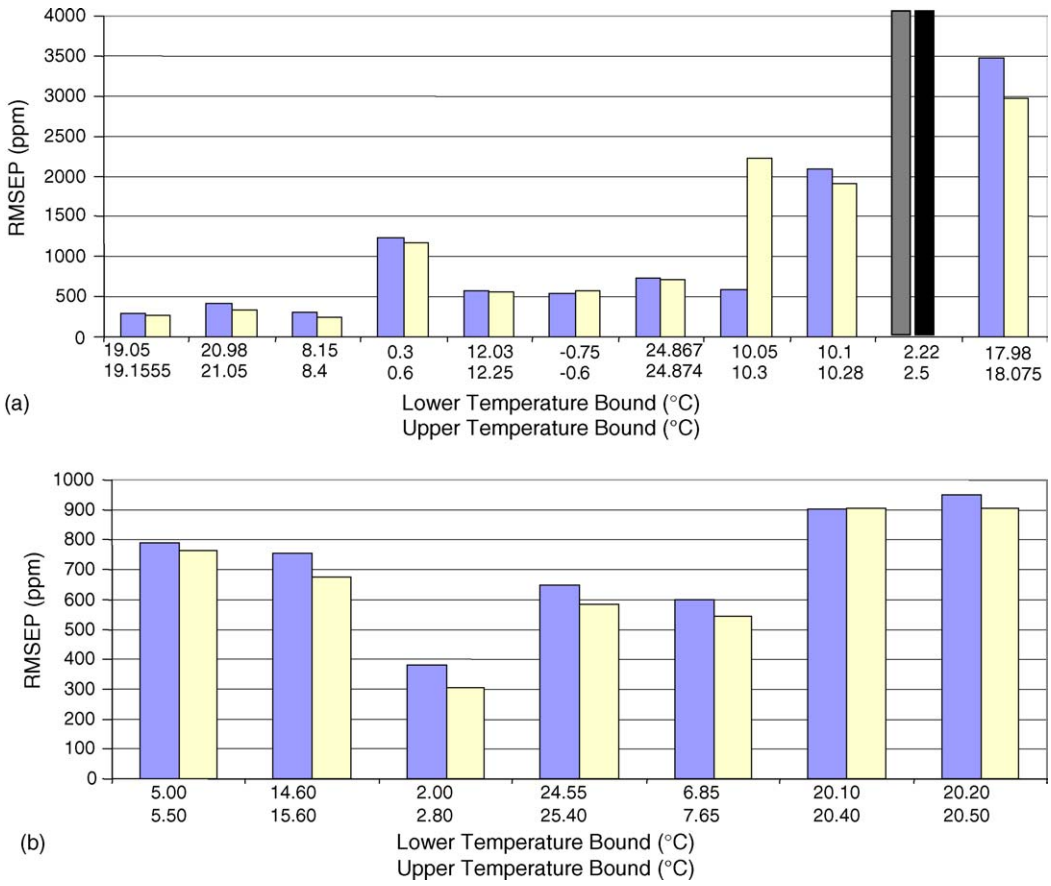

Fig. 7. RMSEP for calibration across 28–48 salinity (a) Experiment 1 with a narrower range of temperatures. (b) Experiment 2 with a wider range of temperatures for each data set. For each graph, the first bar (grey) is RMSEP from single data points, the second bar (white) is RMSEP from a moving average of $n = 10$.

is suspected to be from salt depositing on the sensor at colder temperatures.

4.2. Potential for improvement

A significant part of the initial RMSEP magnitude for a given day is derived from the spectral resolution and signal to noise level of the OceanOptics spectrometer and diode array detector employed. The capability to reproducibly determine the minimum of the SPR spectrum is evident in Fig. 2b when the reproducibility of the λ_{SPR} is compared to the reproducibility of the salinity determined by the conductivity meter. The FO-SPR sensors coupled with the OceanOptics spectrometer employed here is reproducible to $\sim 6 \times 10^{-5}$ refractive index units; comparable to the sensor employed by Liu et al. [26]. Thus, given that the accepted 3×10^{-7} RIU/ppm salinity, we would expect to have prediction errors right at 200 ppm salinity. Coupling the FO-SPR sensors to a 1/4-m spectrometer with a TE cooled CCD camera would offer the advantages of lower detection limits and capability to multiplex to multiple SPR sensors. This has been demonstrated in our laboratory, but not packaged for field portability like the OceanOptics system. The $\sim 3 \times 10^{-6}$ refractive index precision of the larger optical spectrometer should lower the RMSEP to below the 100 ppm precision of the conductivity probe employed as the reference method. If all other sources of errors are accounted, the spectrometer limited RMSEP would be 10 ppm salinity.

The potential to realize such low detection limits can be appreciated when observing the stability of the sensor and the RMSEP when neither the salinity, not the temperature is appreciably changing. Fig. 8 presents these prediction errors for collected at the end of daily experimental collections during experiment 1. Six equilibrium sets were collected over 11 days; the six data sets presented here were collected after the

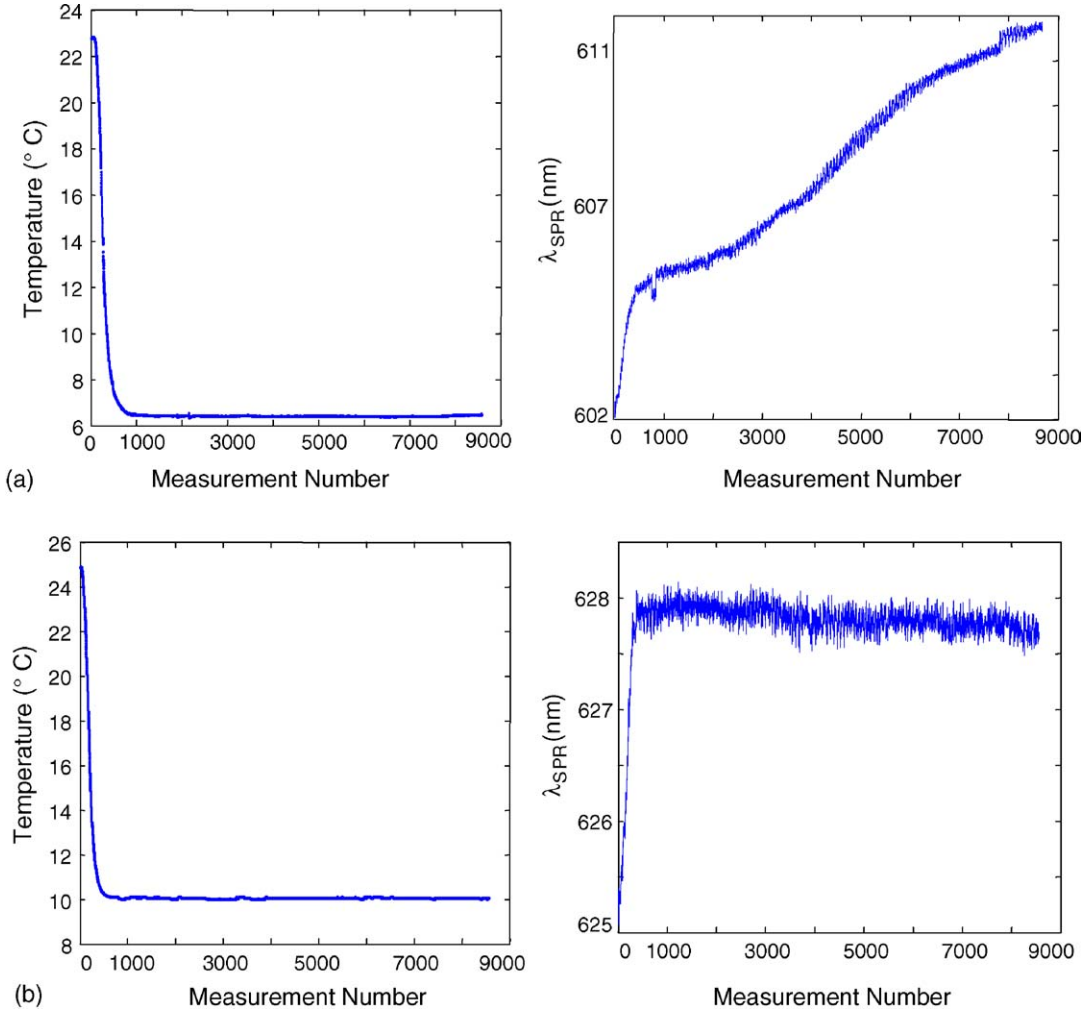

Fig. 9. Temperature and λ_{SPR} data for the first temperature equilibration period in Experiment 1 and a subsequent temperature equilibration period 21 days later. If the temperature and salinity are constant, there should be no appreciable change in λ_{SPR}. The fact (a) is redshifting dramatically suggests its appearance is due to probe drift.

1st, 3rd, 5th, 6th, 10th and 11th data set presented in Fig. 7a. Early in the probes useful life cycle, the sensor is stable to less than 50 ppm. Later in the life cycle, the precision degrades and the sensor eventually fails. The RMSEP for these stability tests track the RMSEP presented in Fig. 7a. For the last two data sets, the SPR probe was beyond the useful lifetime.

4.3. Sensor drift

Obvious in all of this is a problem of sensor drift that must be overcome prior to long-term field deployment. It was observed that a 5–7 day conditioning period was needed before a stable signal would be realized over the course of a 12-h experimental collection. The effect of the sensor fouling can be seen in Fig. 9. A dramatic red shift in the λ_{SPR} is observed during the initial immersion of the sensor into salt water (Fig. 9a). It was determined that about 7 days was required to condition the sensor. Afterwards, the probe would reliably perform for 1–2 weeks. Fig. 7b shows the stability of the sensor, 21 days after initial immersion. Little drift is observed. Eventually the sensor would fail and cease to respond to salinity or temperature changes.

As red shift is indicative of an increase in the local RI around the sensor, it would appear adsorption is occurring on the surface. The system contains deionized water, HDPE, PTFE, Parafilm^{TM} and KCl. Despite the relative inertness of Au, given the possible culprits, KCl is the most likely candidate for adsorption. Chemical attack resulting in the Au layer atrophying would conversely manifest as a blue shift. The mechanism by which KCl adsorption on Au could take place is unknown. SPR cannot "see" RI changed more than 100 nm from the waveguide surface, thus 50 nm of an adsorption layer would render the probe insensitive to salinity changes in the bulk. This may explain the eventual probe demise.

Two options to mitigate the fouling of the sensor are currently under investigation in the laboratory. A popular application of SPR is to sense biological samples by chemically sensitizing the sensor through attachment of relevant functional groups and/or antigens [23,30,31]. As the surface is Au, organothiols readily chemisorb to the surface. Conceivably, organothiols with a hydrophobic tail exposed to the solution would mitigate the adsorption of electrolytes such as $KCl_{(aq)}$. Work in our laboratory has shown the ease and reproducibility with which organothiols can be applied to FO-SPR probes [23]. The potential of using this technique to prolong the lifetime of these FO-SPR probes for use in marine and other electrolytic environments concerns the ongoing work in our laboratory. Characterizing the probes themselves through high-resolution surface sensitive techniques is being explored. Use of an underlayer other than Cr is also being considered. The eventual hope is to prolong FO-SPR sensors' useful lifetime and make them robust for a wide variety of harsh environments not limited to industrial process monitoring and seafloor hydrothermal vents.

5. Conclusion

The FO-SPR sensor presented has demonstrated a sensitivity of <200 ppm to small changes in salinity regardless of temperature, and <300 ppm over a marine-relevant range of salinities regardless of temperature. The probe itself is easily used in situ, is inexpensive to manufacture, and smaller than a conventional conductivity cell. Therefore, its demonstrated ability at several temperatures coupled with its ease of use puts it in the front of the pack of SPR salinity sensors presented to date. Future work will require use of higher accuracy instrumentation to better establish the ultimate sensitivity of the sensor. The sensor drift must be mitigated if not halted in order to make the probe useful for long-term field deployment. Once the higher accuracy calibration is performed and the drift issue properly rectified, this sensor would provide complementary information to conductivity in field marine densitometry, and give an opportunity to monitor salinity in difficult to reach environments.

References

[1] N.P. Fofonoff, J. Geophys. Res. Oceans 90 (1985) 3332.
[2] K. Grasshoff, M.-L. Ehrhardt, K. Kremling, Methods of seawater analysis, second, revised and extended ed, Verlag Chemie, Weinheim, 1983.
[3] E.L. Lewis, R.G. Perkin, J. Geophys. Res. Oceans Atmos. 83 (1978) 466.
[4] R.G. Perkin, E.L. Lewis, IEEE J. Oceanic Eng. 5 (1980) 9.
[5] F.J. Millero, Deep-Sea Research Part I-Oceanographic Research Papers, 2000 47, 1583.
[6] J.S.M. Rusby, Deep-Sea Res. 14 (1967) 427.
[7] R.C. Millard, G. Seaver, Deep-Sea Research Part a-Oceanographic Research Papers, 1990. 37, 1909.
[8] C. Maes, D. Behringer, J. Geophys. Res. Oceans 105 (2000) 8537.
[9] D.V. Hansen, W.C. Thacker, J. Geophys. Res. Oceans 104 (1999) 7921.
[10] M.R. Brininstool, Fiber Optics Ocean Environ. (1990).
[11] E. Augusciuk, A.W. Domanski, M. Roszko, M. Swillo, Proc. SPIE 3731 (1999) 193.
[12] E. Augusciuk, A.W. Domanski, M. Roszko, M. Swillo, Proc. SPIE 3730 (1999) 122.
[13] P.V. Hoi, V.D. Thinh, P.H. An, H.C. Dung, B. Huy, T.T. Cham, Proc. SPIE 3945 (2000) 164.
[14] Y. Zhao, Y.B. Liao, Sens. Actuators B Chem. 86 (2002) 63.
[15] Y. Zhao, B. Zhang, Y. Liao, S. Lai, Proc. SPIE 4920 (2002) 496.
[16] Y. Zhao, Y.B. Liao, B. Zhang, S.R. Lai, J. Lightwave Technol. 21 (2003) 1334.
[17] R.C. Jorgenson, S.S. Yee, Sens. Actuator B Chem. 12 (1993) 213.
[18] R.C. Jorgenson, C.C. Jung, Abstr. Pap. Am. Chem. Soc. 208 (1994) 126.
[19] L.A. Obando, D.J. Gentleman, J.R. Holloway, K.S. Booksh, Sens. Actuators B Chem. 100 (2004) 449.
[20] O. Esteban, M. Cruz-Navarrete, A. Gonzalez-Cano, E. Bernabeu, Appl. Optics 38 (1999) 5267.
[21] O. Esteban, M.C. Navarrete, A. Gonzalez-Cano, E. Bernabeu, Optics Lasers Eng. 33 (2000) 219.
[22] O. Esteban, R. Alonso, M.C. Navarrete, A. Gonzalez-Cano, J. Lightwave Technol. 20 (2002) 448.

[23] J.F. Masson, L.A. Obando, S. Beaudoin, K.S. Booksh, Talanta 62 (2004) 865.
[24] B. Grunwald, G. Holst, Proc. SPIE 3860 (1999) 472.
[25] B. Grunwald, G. Holst, Proc. SPIE 4578 (2002) 96.
[26] D. Liu, Y. Huang, D. Hunag, Proc. SPIE 3897 (1999) 180.
[27] X.H. Quan, E.S. Fry, Appl. Optics 34 (1995) 3477.
[28] L.L. Obando, K.S. Booksh, Anal. Chem. 71 (1999) 5116.
[29] D.J. Gentleman, L.A. Obando, J.F. Masson, J.R. Holloway, K.S. Booksh, Anal. Chim. Acta 555 (2004) 291.
[30] S. Koide, Y. Iwasaki, T. Horiuchi, O. Niwa, E. Tamiya, K. Yokoyama, Chem. Commun. (2000) 741.
[31] K. Kukanskis, J. Elkind, J. Melendez, T. Murphy, G. Miller, H. Garner, Anal. Biochem. 274 (1999) 7.